1

Inverter-based Resource Power Plant Control and AC Delivery

Zhixin Miao and Lingling Fan

Department of Electrical Engineering, University of South Florida, Tampa, FL, USA

1.1 Inverter-based Resource Grid Integration Circuit Topology

AC delivery is a common approach for offshore wind farms (OSWs) located close to shores. As of 2024, the break-even distance to replace an AC delivery system by a DC delivery system is 45 miles [1]. Take the example of the United States' first utility-scale deep-water offshore wind farm – Block Island Wind Farm in Rhode Island. This wind farm has a size of 30 MW and is connected to the mainland power grid through a 25-mile 34.5-kV undersea cable. The wind farm consists of five 6-MW type-4 wind turbines (GE/Alstom Haliade 150-6 MW offshore wind turbine) with direct-drive permanent magnet generators. Each tower base has a wind turbine (including the mechanical parts, a generator, and an inverter of 900 V), a pad-mount transformer to step 900 V to 34.5 kV, switchgear, and a low-voltage electrical distribution cabin.

In the Rock Island Wind Farm case, 34.5-kV or medium-voltage (MV) cables are used to transmit 30 MW of power. To transmit power greater than 100 MW, high-voltage (HV) AC delivery system is preferred. The newly operational 132-MW South Fork Wind Farm, 19 miles away from Block Island and 30 miles east of Montauk Point on the South Fork of New York's Long Island, uses a 138-kV undersea cable to deliver power to an onshore 138/69-kV substation at Long Island. An offshore substation was built to connect with twelve 11-MW Siemens Gamesa type-4 wind turbines through MV cables of 34.5–66 kV. The offshore substation has step-up transformers to boost voltage to 138 kV. In addition, the substation is equipped

Weak Grid Integration of Offshore Wind: Challenges and Control Solutions, First Edition.
Zhixin Miao and Lingling Fan.
 Published 2026 by John Wiley & Sons, Inc.

with switchyard reactors, a small diesel generator, and a supervisory control and data acquisition system to monitor and control wind farm operations.

OSW construction in the United States lags behind Europe. Many experiments and guides have been produced from the prior installation. For example, CIGRE Technical Brochure 483 "Guidelines for the Design and Construction of AC Offshore Substations for Wind Power Plants" [2] published in 2011. This 378-page guide extensively covers OSW substation construction, including the justification of voltage levels. For OSWs, the transmission level is usually from 132 to 150 kV for 100 MW-size OSWs, with 245-kV AC level gaining importance for 350/400 MW OSWs. On the other hand, 400-kV AC level does not seem to have a promising future due to cable manufacturing capability and 400-kV switchgear and transformers being too bulky.

1.2 Inverter-level Control Logic

The focus of the book is on the operational challenges of inverter-based resource (IBR) power plants integrated into weak AC grids. Therefore, only the most relevant controls are examined. These include the inverter-level control and power plant-level control.

From the grid's point of view, a solar PV, a type-4 wind turbine, and a battery energy storage system (BESS) have very similar characteristics. All are connected to AC grids through a grid-connected inverter, and the inverter's control dynamics influences the system dynamics. While all types of inverter controls are of similar nature and can be categorized as grid-following control, it has to be noted that original equipment manufacturers (OEMs) are different. In the United States, SMA and Tesla are two main OEMs for solar and battery inverters, while GE and Siemens are the main OEMs for wind turbine inverters.

Compared to an AC machine, an inverter is very sensitive to overcurrent. Therefore, effective current limiting technologies have been developed to ensure that inverter currents are within limits. This is usually achieved by having tight inner current control so that the current measurements can follow the current order. Limits can be added to the current orders. When designed properly, an inverter indeed acts as a current source.

Besides the inner current control, an inverter has the outer control to achieve control functions, e.g., power or voltage regulation. And also, very importantly, an inverter needs to have a synchronizing unit to be integrated into a main grid. In the following, the three control units – synchronizing units, inner current control, and outer grid function control – will be explained one by one.

Figure 1.1 shows the circuit diagram of an IBR grid integration system. The converter current i and the point of common coupling (PCC) bus voltage v_{PCC} or v will be measured and used for IBR control. The outputs from the IBR control are the

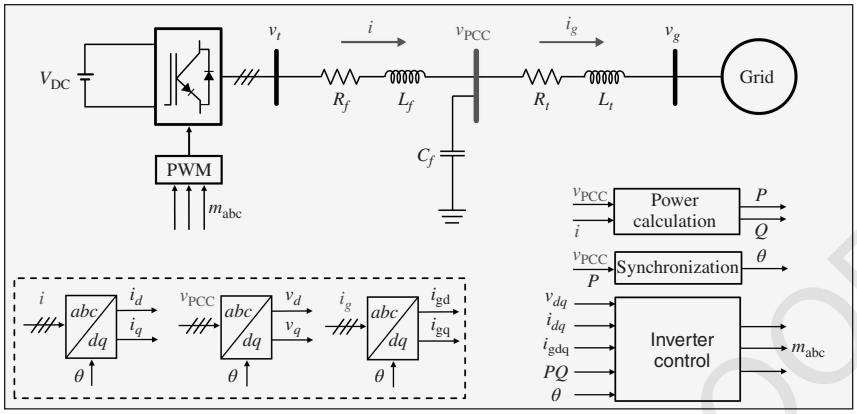

Figure 1.1 An IBR grid integration system with the measurements for IBR control marked.

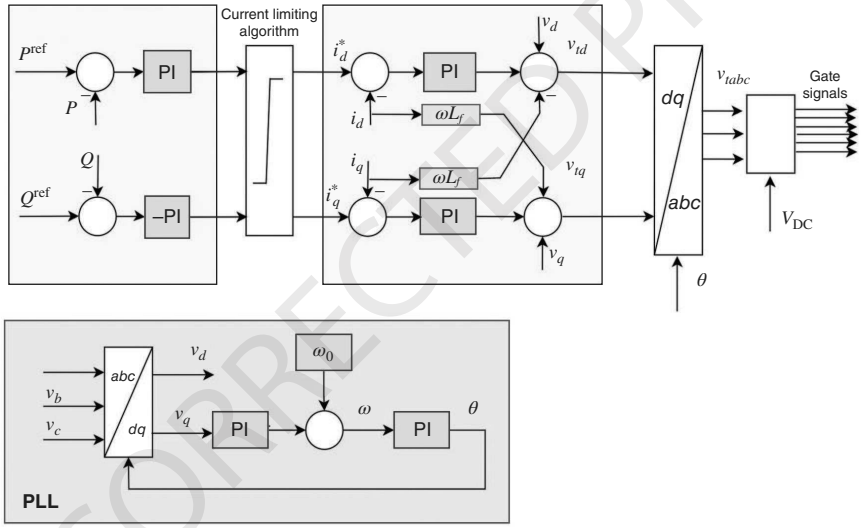

Figure 1.2 Inverter-level grid-following control structure.

modulation signals m_{abc} that influence the terminal voltage of the voltage-source converter, denoted as v_t, where $v_{t\phi} = m_\phi \frac{V_{DC}}{2}$, and $\phi = a, b, c$.

Figure 1.2 shows a typical grid-following (GFL) control structure with three units, where a phase-locked loop (PLL) generates a synchronizing angle, the inner current control regulates the dq currents, and the outer control regulates the real and reactive power.

1.2.1 Inner Current Control

It is easier to regulate DC signals than AC signals. In addition, we will show that current vector control relies on regulating *dq* components of the current space vector. When the current space vector is viewed in the static frame, it is a rotating vector. When the current space vector is viewed from the PLL frame, it is a static vector at steady state, and its *dq* components in the PLL frame are DC signals. Therefore, the inner current control is typically implemented in the PLL frame to ensure that the *dq* currents follow the current references generated by the outer control loop.

It can be seen that the IBR's output current $\vec{i}$ has the following relationship with the converter voltage $\vec{v}_t$ and the PCC bus voltage $\vec{v}$, viewed in the static frame:

$$\vec{v}_t - \vec{v} = (R + Ls)\vec{i}, \tag{1.1}$$

where R and L are the resistance and inductance of the choke filter, respectively. In the PLL frame with a rotating speed of ω, the above relationship becomes the following:

$$v_{td} + jv_{tq} - (v_d + jv_q) = (R + L(s + j\omega))(i_d + ji_q), \tag{1.2}$$

$$\Longrightarrow (R + Ls)(i_d + ji_q) = \underbrace{v_{td} + jv_{tq} - (v_d + jv_q) - j\omega L(i_d + ji_q)}_{\overline{u}} \tag{1.3}$$

$$(R + Ls)i_d = \underbrace{v_{td} - v_d + \omega L i_q}_{u_d} \tag{1.4}$$

$$(R + Ls)i_q = \underbrace{v_{tq} - v_q - \omega L i_d}_{u_q}. \tag{1.5}$$

The inner current control treats i_d (or i_q) as the output from the plant or the measurement to be compared with the order i_d^* (or i_q^*). The error between the order and the measurement is then fed to a PI controller to generate the output. This output is $u_d = v_{td} - v_d + \omega L i_q$ (or $u_q = v_{tq} - v_q - \omega L i_d$). To arrive at the converter voltage signals v_{td} (or v_{tq}) that can be used to change the converter voltage, the output should be compensated by a feedforward unit of the PCC bus voltage v_d (or v_q) and a cross-coupling unit $-\omega_L i_q$ (or $\omega_L i_d$).

It can be seen that the current order and the current measurement have the following relationship:

$$\underbrace{\left(K_p + \frac{K_i}{s}\right)}_{G_{\mathrm{PI}}}(\bar{I}^* - \bar{I}) = \overline{u} = (R + Ls)\bar{I}. \tag{1.6}$$

Therefore, the closed-loop system of the measurement tracking the order is expressed as follows:

$$\frac{\Delta\bar{I}}{\Delta\bar{I}^{*}} = \frac{G_{\mathrm{PI}}}{G_{\mathrm{PI}} + R + Ls} = \frac{K_p s + K_i}{Ls^2 + (R + K_p)s + K_i}. \tag{1.7}$$

Figure 1.3 shows the Bode diagrams of the closed-loop system for different K_p. It can be seen that K_p is very sensitive to the bandwidth. A quick evaluation of the bandwidth can be taken by approximating the closed-loop transfer function:

$$\frac{\Delta\bar{I}}{\Delta\bar{I}^{*}} = \frac{1}{1 + \frac{R+Ls}{\frac{K_i}{s}+K_p}} \approx \frac{1}{1 + \frac{L}{K_p}s}. \tag{1.8}$$

Since the current control design requires having a very high bandwidth above 100 Hz, and at the high-frequency region, $|Ls| \gg R$ and $K_p \gg \left|\frac{K_i}{s}\right|$, the closed-loop system can be approximated as a first-order low-pass filter and its rise time is $\frac{L}{K_p}$.

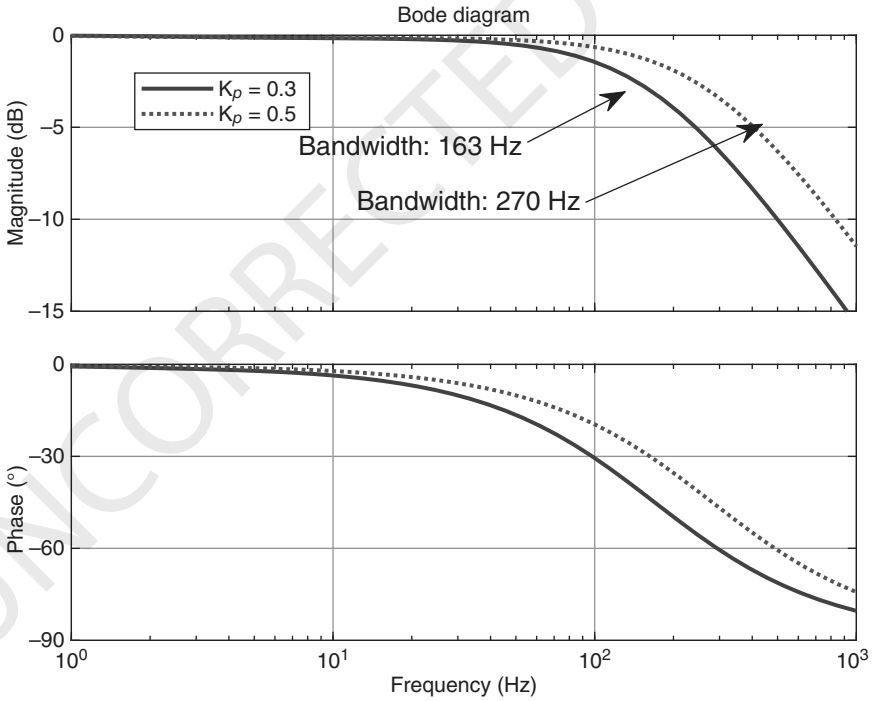

Figure 1.3 Current tracking performance. $K_i = 5$, $L = 0.108/(120\pi)$, $R = 0.01$.

Its bandwidth is $\frac{K_p}{L}$ rad/s. Increasing K_p from 0.3 to 0.5 effectively improves the controller's bandwidth by 1.7 times. This evaluation agrees with the bandwidths shown in the Bode diagrams in Figure 1.3: for the PI controller of $0.3 + 5/s$, the current tracking control's bandwidth is 163 Hz, while for the PI controller of $0.5 + 5/s$, the bandwidth is 270 Hz.

The inner current controller consists of three elements: the PI controllers, the cross-coupling terms, and the PCC voltage feedforward. This control structure has been presented in the classic book [3].

The cross-coupling terms were introduced in three-phase motor drives, to counter the coupling effect of the plant model (the RL circuit dynamics in a *dq* frame). This coupling effect can be shown as the terms with imaginary coefficients in the complex vector expressions for voltage and current in the *dq* frame. For example,

$$\bar{V}_t - \bar{V} = (R + Ls)\bar{I} + j\omega L\bar{I}. \tag{1.9}$$

Reference [4] has compared three types of designs for a motor serving an RL load: just PI controllers, the PI controllers with cross-coupling, and the complex vector controller in the form of $K_p + \frac{K_i s + jK_p\omega}{s}$. The first one (just PI controllers) shows degraded performance if the rotating speed of the *dq* frame is close to the controller bandwidth. The latter two achieve similar performance for different *dq* frame speeds, since the introduced cross-coupling terms can effectively counter the coupling from the plant.

One shortcoming of the strategy of using PI controller with cross-coupling is that it requires an accurate estimation of the choke filter's inductance. Reference [4] shows that if the inductance parameter deviates significantly from its actual real value, the controller's performance will deteriorate. On the other hand, the complex vector controller does not need this info and the controller's performance is robust against this parameter variation.

In AC motor drives, voltage feedforward is usually not used. This unit was introduced specifically for grid-connected converter control. The technology may be traced back to [5], a paper published in 2004. Including PCC voltage feedforward renders the inverter immune to grid disturbances and allows it to function as a current source.

Figure 1.2 shows a typical grid-following control structure, which consists of the outer control, the inner current control, and the synchronizing unit (a PLL). The typical PI controller for the outer control is $0.25 + 25/s$, for the inner current control $0.5 + 5/s$, while the PLL's PI control is $60 + 1400/s$. It is worthwhile noting that all those are based on per-unit measurements.

1.2.2 Synchronizing Units: Grid-following Versus Grid-forming

There are mainly two types of inverter control: GFL and grid-forming (GFM). In terms of operation, a grid-following IBR cannot serve a load as the only source, while a grid-forming IBR has such capability. This is due to the fact that the grid-following type lacks the capability to generate a stable frequency. It tracks the system's frequency. On the other hand, a grid-forming type has the capability to generate a stable frequency and operate as the only source. It can also be synchronized to a system with other sources. Therefore, a grid-following IBR does not have the capability of black start, while a grid-forming IBR has such capability.

In control design, the key difference between the two types is how each realizes synchronism and generates frequency. The grid-following converter relies on voltage-based synchronization, which is also called as PLL. The PLL has three-phase voltage as the input and outputs an angle and a frequency. A PLL can either be viewed as a sensor or be used as a controller, since the PLL's output angle can be used as a synchronizing angle. On the other hand, grid-forming control relies on power-based synchronization. The synchronizing angle and frequency are generated either through power–frequency droop control or a control block emulating the swing dynamics of a synchronous generator.

1.2.2.1 GFL: Voltage-based Synchronization

In the majority of bulk power system-connected IBRs, a PLL is used as the synchronizing unit. The initial use of PLL in high-voltage transmission systems may have been in flexible AC transmission systems (FACTS) and high-voltage direct current (HVDC) systems. PLLs are for synchronization. STATCOMs rely on PLLs for synchronization with the main grid and generate reactive current. HVDC's inverters and rectifiers also rely on PLLs for synchronization with the interfacing AC grids. While the terminology PLL has been mentioned in Hingorani's book *Understanding FACTS: Concepts and Technology of Flexible AC Transmission Systems* [6], the detailed PLL technology has not been covered. PLL has been thoroughly covered in a 2003 paper "Phase Locked Loop System for FACTS" by Dragan Jovcic [7].

A fundamental knowledge is that a set of three-phase signals can form a rotating space vector through algebraic manipulation. This concept comes from physics. In AC machines, three-phase sinusoidal currents flowing through stator windings form a rotating magnetic field of a constant magnitude with the same speed as the frequency. So the effect of a set of AC currents forming a rotating magnetic field is the same as a DC current flowing in the rotor winding, with a magnitude 1.5 times the per-phase AC current amplitude. The underlying requirement for the current set is that this is a balanced set, or a positive-sequence set. In AC machines, the geometric placement of the stator windings ensures that the reference axis for each phase is different, with the b-axis leading the a-axis by 120°, and the c-axis leading

the b-axis by 120°. Therefore, the equivalence between the three-phase AC current and the DC current on a rotating frame can be established as:

$$\frac{3}{2}\hat{i}_a e^{j\theta_a} = i_a + e^{j\frac{2\pi}{3}} i_b + e^{-j\frac{2\pi}{3}} i_c, \tag{1.10}$$

if $i_a = \hat{i}\cos(\theta_a)$, $i_b = \hat{i}\cos(\theta_a - \frac{2\pi}{3})$, and $i_c = \hat{i}\cos(\theta_a + \frac{2\pi}{3})$.

The space vector is defined to have the analytical form of i_a, or v_a:

$$\vec{i} = \frac{2}{3}\left(i_a + e^{j\frac{2\pi}{3}} i_b + e^{-j\frac{2\pi}{3}} i_c\right), \tag{1.11}$$

$$\vec{v} = \frac{2}{3}\left(v_a + e^{j\frac{2\pi}{3}} v_b + e^{-j\frac{2\pi}{3}} v_c\right). \tag{1.12}$$

With the objective of tracking the angle of a voltage space vector, the key idea of a three-phase PLL is to ensure that the PLL's angle or the frame generated by the PLL aligns with the voltage space vector. In other words, the error between θ_a and θ generated by the PLL should be 0. This can be achieved by enforcing the quadratic component of the projection of the voltage space vector on the PLL frame to be 0. This quadratic component can be expressed as:

$$\begin{aligned} v_q &= \text{Imag}\left\{\vec{v}\, e^{-j\theta}\right\} \\ &= \text{Imag}\left\{\tfrac{2}{3}\left(v_a e^{-j\theta} + e^{-j\left(\theta-\frac{2\pi}{3}\right)} v_b + e^{-j\left(\theta+\frac{2\pi}{3}\right)} v_c\right)\right\} \\ &= \tfrac{2}{3}\begin{bmatrix} -\sin\theta & -\sin\left(\theta-\frac{2\pi}{3}\right) & -\sin\left(\theta+\frac{2\pi}{3}\right)\end{bmatrix}\begin{bmatrix} v_a \\ v_b \\ v_c\end{bmatrix}. \end{aligned} \tag{1.13}$$

To enforce a zero v_q, a proportional integral (PI) controller may be used to generate the frequency. Further, the frequency is integrated to generate the angle θ, which is fed to the *abc/dq* conversion in Equation (1.13) to generate v_q. It can be seen that a PLL adopts feedback control to achieve the objective of angle tracking.

It can be seen that $v_q = \text{Imag}\left\{\vec{v}e^{-j\theta}\right\} = \text{Imag}\left\{\hat{v}e^{j(\theta_a-\theta)}\right\} = \hat{v}\sin(\theta_a - \theta)$. In the per-unit system, the voltage amplitude can be assumed to be close to 1 pu under normal operating conditions. For small disturbance conditions $\sin(\theta_a - \theta) \approx \theta_a - \theta$. Therefore, the PLL can be viewed as a second-order linear feedback system. The input to the PI controller is the angle difference $(\theta_a - \theta)$, and the output of the PI controller is further passed through an integrator to generate the angle θ. The open-loop gain and the closed-loop system can be seen as follows:

$$\begin{aligned} G_{\text{open}} &= \frac{\theta}{\theta_a} = \frac{K_p s + K_i}{s}\frac{1}{s}, \\ G_{\text{closed}} &= \frac{G_{\text{open}}}{1 + G_{\text{open}}} = \frac{K_p s + K_i}{s^2 + K_p s + K_i}. \end{aligned} \tag{1.14}$$

The closed-loop system behaves as a second-order low-pass filter. For a PI gain set of (60, 1400), the closed-loop system has a bandwidth of 13 Hz.

1.2.2.2 GFM: Power-based Synchronization

The voltage-based synchronization requires a stiff PCC bus voltage and generates a frame that aligns or follows the PCC bus voltage. Implicitly, a strong grid is required to have a stiff PCC bus voltage. At weak grid conditions, as reported in [8], PLLs may experience large angle deviations or a loss of synchronism during a dip in the grid voltage. Additionally, this synchronizing mechanism lacks the capability to regulate real power according to the frequency. Therefore, a different synchronizing scheme is desired for weak grid operations.

The power-based synchronization is very similar to the operation of a synchronous generator. In particular, power–frequency droop control has been used in inverters in a standalone system to share loads. In the early 2000s, when distribution generators (DGs) became a research topic, the operation of multiple DGs (many of them are inverter-based) was researched. In the early 2000s, Robert Lasseter led the Consortium for Electric Reliability Technology Solutions (CERTS) Microgrid, a major US Department of Energy research initiative that advanced microgrid technology from theory into practice. The CERTS Microgrid Test Bed located at the AEP Dolan Technology Center in Ohio can demonstrate seamless transition between grid-connected and islanded modes. Lasseter designed single-loop inverter control with each inverter acting as a voltage source with power–frequency droop-based synchronization [9].

Figure 1.4a shows a simple power–frequency droop controller that generates a synchronizing angle. Based on the control logic, the angle can be expressed as follows:

$$\theta = \underbrace{\int R\omega_0(P^* - P)dt}_{\delta} + \omega_0 t, \tag{1.15}$$

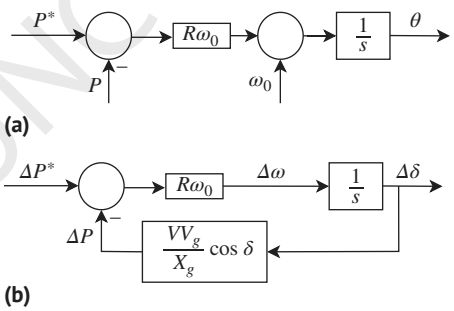

Figure 1.4 (a) Power–frequency droop control. (b) The linear feedback system.

where P^* is the real power order, P is the real power measurement, and R is the droop parameter in per unit. If $R = 0.05$, this means that for a 1 pu change in real power, there will be a 5% change in frequency or a 3 Hz change in a 60 Hz system. When an IBR acts as a voltage source and connects to an infinite bus (a constant voltage source with a magnitude of V_g and an angle of $\omega_0 t$) through a reactance X_g, the real power expression can be simply written as:

$$P = \frac{VV_g}{X_g} \sin \delta, \tag{1.16}$$

where V is the PCC bus voltage magnitude, and δ is the angle difference between the IBR and the grid. Both V and V_g can be assumed as 1 pu in analysis. It can be seen that the droop control and the above equation form a negative feedback system. The linearized system is shown in Figure 1.4b. This system is stable as long as the angle difference between the two sources is within the limit of $[-90°, 90°]$.

Figure 1.5a shows the responses of the real power measurement upon a 10% change in P^* for three cases: $X_g = 0.1$, $X_g = 0.2$, and $X_g = 0.5$. In all three cases, the initial power exporting level is 1 pu. The initial values of δ are $\sin^{-1}0.1$, $\sin^{-1}0.2$, and $\sin^{-1}0.5$ for the three cases. It can be seen that when the grid is weak (or X_g is large), the response of power becomes slower. Figure 1.5b shows the frequency responses of $\Delta P/\Delta P^*$, which acts as a low-pass filter. It can be seen that 5% droop parameter and $X_g = 0.5$ lead to a bandwidth of 5 Hz.

1.2.3 Outer Control Functions

1.2.3.1 Real and Reactive Power Regulation Through Current Vector Control in GFL

Real and reactive power regulation is a common control objective for IBRs. This is usually realized through decoupled current vector control. This technology evolves from AC motor drives, where a cascaded control structure is usually adopted, with the inner current control offering tight current regulation and outer control offering flux and torque regulation. The stator's current space vector is decomposed into two orthogonal components: the component related to the flux and the component related to the torque. For flux regulation, the flux-related component is to be adjusted, while for torque regulation, the torque-related component is to be adjusted. In grid-tied inverters, real and reactive power have corresponding current components: the real and the reactive currents. This requires that the current space vector be projected onto a frame aligned with the voltage space vector. The real current aligns with the voltage space vector and is notated as i_d. The reactive current is orthogonal to the voltage space vector and is notated as $-i_q$ if

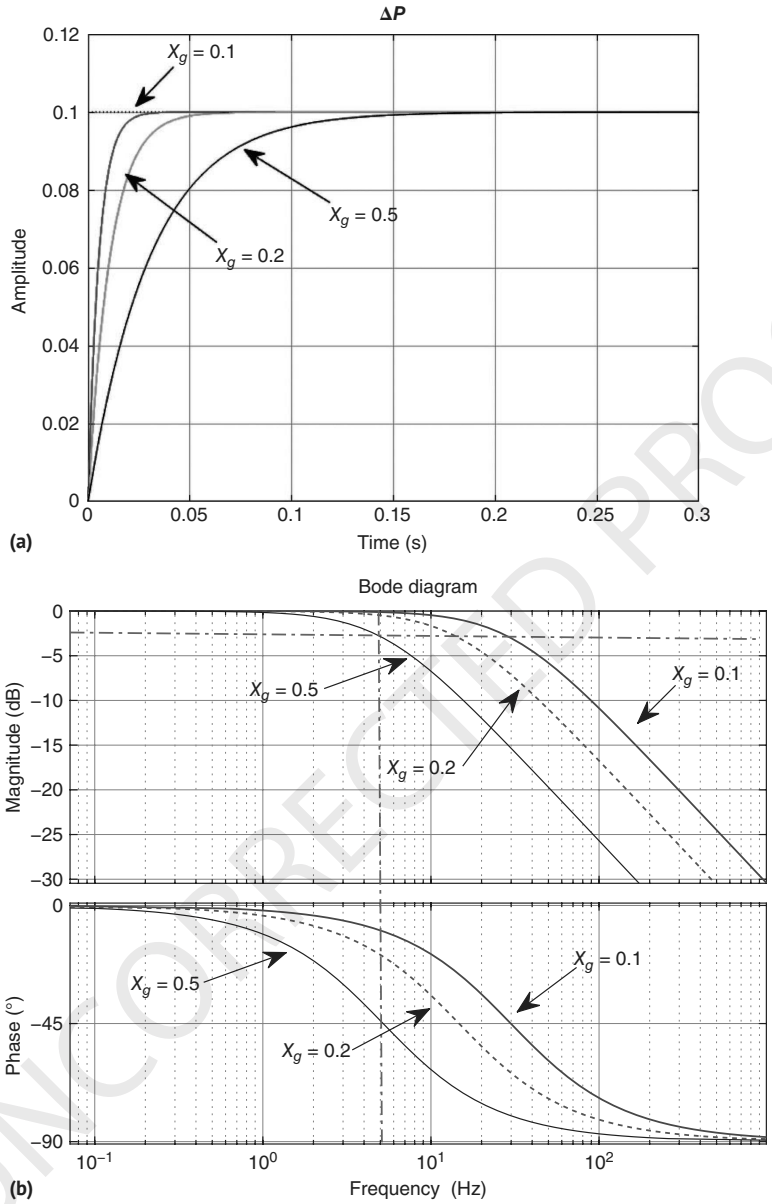

Figure 1.5 Power–frequency droop-based synchronization. (a) Bode diagrams of the closed-loop system. (b) Step responses of the closed-loop system.

the q-axis leads the d-axis. The frame aligned with the voltage space vector can be set up by the PLL.

$$S = P + jQ = \bar{V} \cdot \bar{I}^* = V(i_d + ji_q)^* = \underbrace{V \cdot i_d}_{P} + j\underbrace{V \cdot (-i_q)}_{Q}. \tag{1.17}$$

Based on the simple relationship between P and i_d (Q and $-i_q$), a PI controller can be designed for power regulation. The outputs of the PI controllers are the dq current orders. Since inverters have tight current controls, their current orders are viewed to be the same as their current measurements. In the per-unit system, voltage is usually kept at 1 pu. Therefore, $P \approx i_d$ and $Q \approx -i_q$. For a PI controller with an input defined as the difference between the reference and the measurement, the closed-loop transfer function is given by:

$$G = \frac{K_p + K_i/s}{1 + K_p + K_i/s} = \frac{\frac{K_p}{K_i}s + 1}{\frac{1+K_p}{K_i}s + 1}. \tag{1.18}$$

This is a low-pass filter with the time constant approximately $\frac{1+K_p}{K_i}$. For a set of PI gains (0.25, 25), the resulting time constant or rising time is 0.05 s. This controller has a bandwidth of 3 Hz. For a set of the PI gains (1, 100), the resulting rising time is 0.02 s and the bandwidth is about 8 Hz. The outer control can have variations. For example, the d-axis control may be used to regulate the DC-link voltage instead of real power. Similarly, the q-axis control may be used to regulate the AC voltage instead of reactive power.

1.2.3.2 Outer Control Functions in GFM

In Chapter 3, a variety of GFM control strategies will be elaborated. In this chapter, a brief overview of GFM's outer control functions and their design is given. We may start from the typical GFL control diagram shown in Figure 1.2 and examine how to retrofit the GFL into a power synchronization-based GFM.

In the GFL, the PLL has two functions: generating a synchronizing angle and aligning the synchronizing frame's d-axis with the PCC bus voltage space vector. A power-based synchronizing unit has the capability of generating the synchronizing angle, while lacking the capability of frame alignment. Therefore, this second control function should be taken care of by the GFM's outer control. In a PLL, frame alignment is achieved by enforcing the projection of the PCC bus voltage on the q-axis (v_q) to 0. Similarly, in the GFM's outer control, v_q may be used as an input to a PI controller, which generates the current orders in the dq frame. The question is: which current order, i_d^* or i_q^*, should be generated? It can be seen that i_d or the real current injection influences the PCC bus voltage angle, while i_q or the reactive current injection mainly influences the PCC bus voltage magnitude.

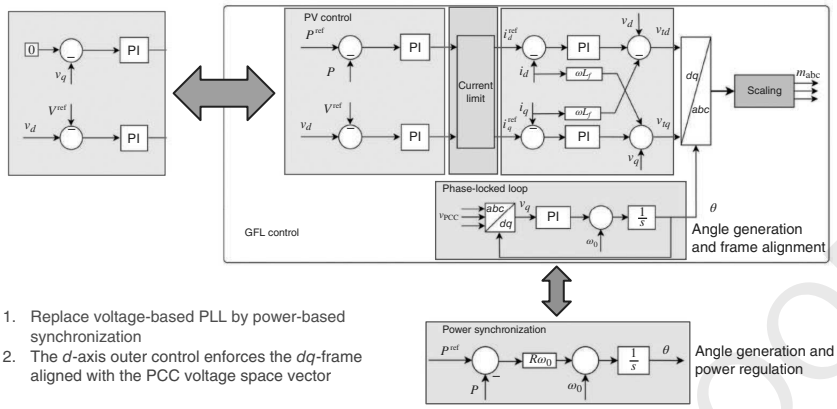

Figure 1.6 Retrofitting a GFL to a GFM.

Therefore, the d-axis outer control in a GFM should be used for frame alignment, while the q-axis outer control generates i_q^*.

In the GFL, real power regulation is conducted by the d-axis control. This function is achieved by the power-based synchronization control. The aforementioned retrofitting procedure leads to a GFM design. In Chapter 3, the design is presented as the multi-loop GFM with vector current control.

Figure 1.6 presents a comparison between the GFL and the GFM, where the PLL is replaced by the P–f control and the d-axis power regulation is replaced by the v_q control.

1.3 Power Plant-level Control Logic

A solar PV power plant or a wind farm usually has hundreds of inverters. The plant-level control is usually located at the point of interconnection (POI). This control center takes in the measurements from the POI, e.g., voltage and frequency, and outputs hundreds of commands to the inverter-level controls, e.g., reactive power orders and real power orders, through communication links. The latency of communication systems ranges from 100 ms to several seconds.

Figure 1.7 shows the circuit topology of a solar PV power plant, which includes both solar PVs and a battery energy storage system (BESS). Individual IBRs with a voltage level of 480 V are connected to 34.5-kV cables through transformers, and further to a 230 kV transmission grid. Measurements at the POI are taken for plant-level control, while measurements at the individual IBR terminals are taken for inverter-level control. Typical plant-level and inverter-level controls are shown in Figure 1.8.

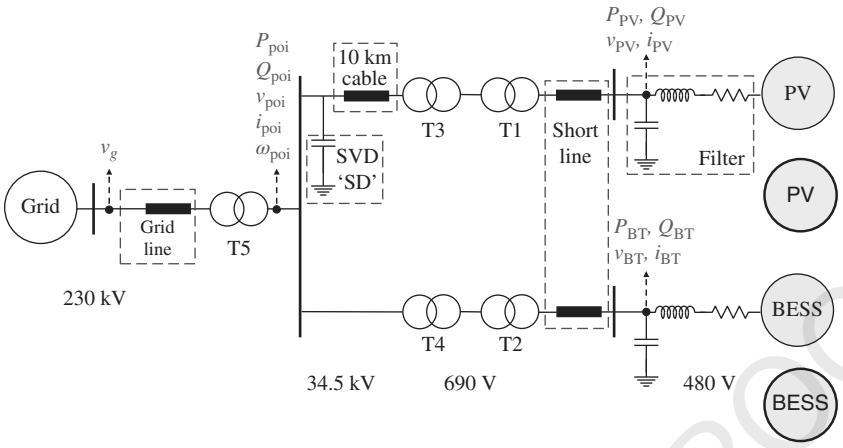

Figure 1.7 Circuit topology of a solar PV plus battery energy storage system power plant.

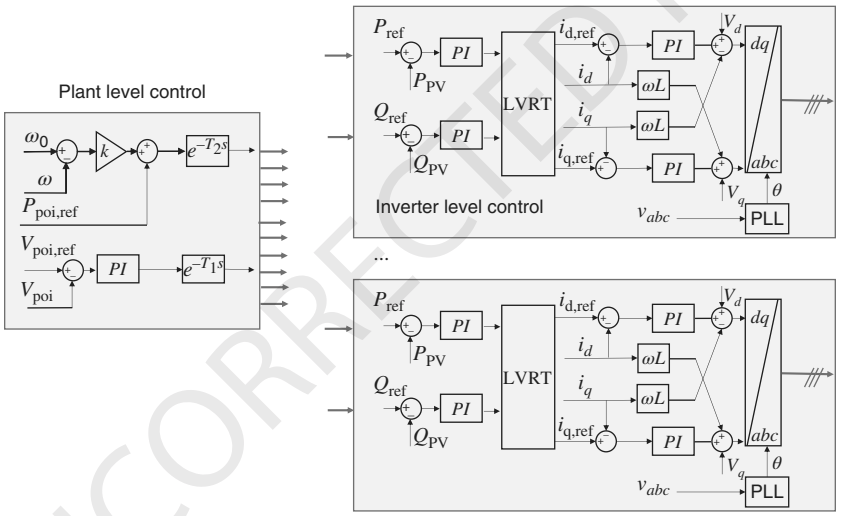

Figure 1.8 Plant-level control and inverter-level control.

In the plant-level control, for the frequency-droop control, the typical value of the droop (power to frequency) is 5% pu/pu. This means that if there is a 1 pu change in power, there will be a 5% pu (or 3 Hz) change in frequency. To implement this droop value into the frequency-to-power block, the gain should be 20 pu/pu. In case, the measured frequency is in the physical unit of rad/s, then the gain should be $20/(120\pi)$ pu/(rad/s).

For the voltage-reactive power control block, if proportional control is assumed, this becomes V–Q droop control. A typical value is to ensure that a 1% decrease in voltage results in 5–10% increase in reactive power. Therefore, the V–Q droop parameter is 5–10 pu/pu. In the case where a PI controller is used, a typical control can be set as $2 + 10/s$.

1.4 Study Methods: Analysis and Electromagnetic Transient Simulation

Throughout this book, we build testbeds in an electromagnetic transient (EMT) simulation environment, e.g., MATLAB Simscape's Specialized Power Systems and PSCAD. EMT computer simulation provides high-fidelity simulation results comparable to the real world. Instead of conducting circuit-based experiments in a lab by connecting components and configuring controls in hardware, EMT simulation enables us to have a virtual lab with a GUI interface, so we can build circuits by finding components in its library, connecting components, and placing scopes to have a circuit with monitors, and further configuring the controllers of IBRs to check a testbed's performance upon dynamic events, e.g., line tripping, voltage dipping, etc. A more detailed description of EMT simulation and a step-by-step guide can be found in the authors' book [10].

With computer simulation as the test and validation tool, the main analytical technique that this book adopts is the fundamental dynamical system analysis, including frequency-domain modeling and analysis. In this chapter, we have already used these fundamental systems and control techniques to examine the characteristics of a PLL, power–frequency control, and outer and inner current control design.

1.5 Summary

This chapter describes the control logics deployed in IBR power plants. The focus is on the control logics used in the grid-connected inverters and the control logics used in the plant-level control. This lays the foundation for the forthcoming discussion in Chapter 2, where the challenges of IBRs operating in weak grids will be examined. Those challenges are closely related to the control logics. Also, the design principles of the control units will be visited repeatedly in Chapter 2.

References

1 J. Fu and S. Shah, Offshore transmission: Key to unlocking wind energy from oceans [guest editorial], IEEE Power and Energy Magazine, vol. 22, no. 5, pp. 17–19, 2024.

2 Conseil international des grands réseaux électriques. Comité d'études B3, *Guidelines for the design and construction of AC offshore substations for wind power plants*. Cigré, 2011.
3 A. Yazdani and R. Iravani, *Voltage-sourced converters in power systems: modeling, control, and applications*. John Wiley & Sons, 2010.
4 F. Briz, M. W. Degner, and R. D. Lorenz, Analysis and design of current regulators using complex vectors, IEEE transactions on Industry Applications, vol. 36, no. 3, pp. 817–825, 2002.
5 Y. Li, D. Vilathgamuwa, and P. C. Loh, Design, analysis, and real-time testing of a controller for multibus microgrid system, IEEE Transactions on Power Electronics, vol. 19, no. 5, pp. 1195–1204, 2004.
6 N. Hingorani and L. Gyugyi, *Understanding FACTS: Concepts and technology of flexible AC transmission systems*. Wiley, 2000. https://books.google.com/books?id=2-ceAQAAIAAJ
7 D. Jovcic, Phase locked loop system for facts, IEEE Transactions on Power Systems, vol. 18, no. 3, pp. 1116–1124, 2003.
8 Reliability Guideline, NERC *Integrating inverter based resources into low shortcircuit strength systems,* North American Electric Reliability Corporation, Tech. Rep., 2017.
9 R. H. Lasseter, J. H. Eto, B. Schenkman, J. Stevens, H. Vollkommer, D. Klapp, E. Linton, H. Hurtado, and J. Roy, Certs microgrid laboratory test bed, IEEE Transactions on Power Delivery, vol. 26, no. 1, pp. 325–332, 2011.
10 L. Fan and Z. Miao, *Modeling and stability analysis of inverter-based resources*. CRC Press, 2023.